Declining Snowpack in the Presence of Stable Precipitation May Not Negatively Impact Baseflow or Floodplain Vegetation in the Middle Fork Rock Creek Watershed, Montana, USA

Emily Iskin[1], Anna Bergstrom[2], and Jodi Brandt[1]

[1] Human-Environment Systems, Boise State University, Boise, ID 83725
[2] Department of Geosciences, Boise State University, Boise, ID 83725

Abstract

In the age of snow droughts and megafires, water availability and changes in precipitation, snowpack, and baseflows are active areas of research. Headwater streams are where all large rivers begin, but their seasonal water availability is difficult to measure because they are so abundant and remote. Remote sensing can help monitor small streams semi-arid areas if there is an appropriate proxy for water availability given the coarse spatial resolution of satellite data. In this study, 40 water years (1984-2024) of climate, streamflow, and floodplain vegetation data are compiled in the relatively undisturbed and gaged Middle Fork Rock Creek watershed in Montana to investigate if and how climate, streamflow, and vegetation are changing through time and/or are correlated with each other. We find that temperatures are warming, snowpacks are shrinking, and total flow volume is growing, but total precipitation, late season baseflow volume, and floodplain vegetation remain stable. In a given water year, greater coverage of floodplain vegetation in September is correlated with more precipitation and higher late season baseflow volume, indicating that the stream and the vegetation might not be in direct competition for available water. Additionally, floodplain vegetation measured with remote sensing is likely an appropriate proxy for late season baseflow in this watershed and could potentially be used to monitor ungaged watersheds. More study is needed to determine if floodplain vegetation is an appropriate proxy for water availability generally across the semi-arid U.S.,; and how these relationships between climate, streamflow, and vegetation might vary across watersheds of varying size, topography, and ecoregion.

Graphical Abstract

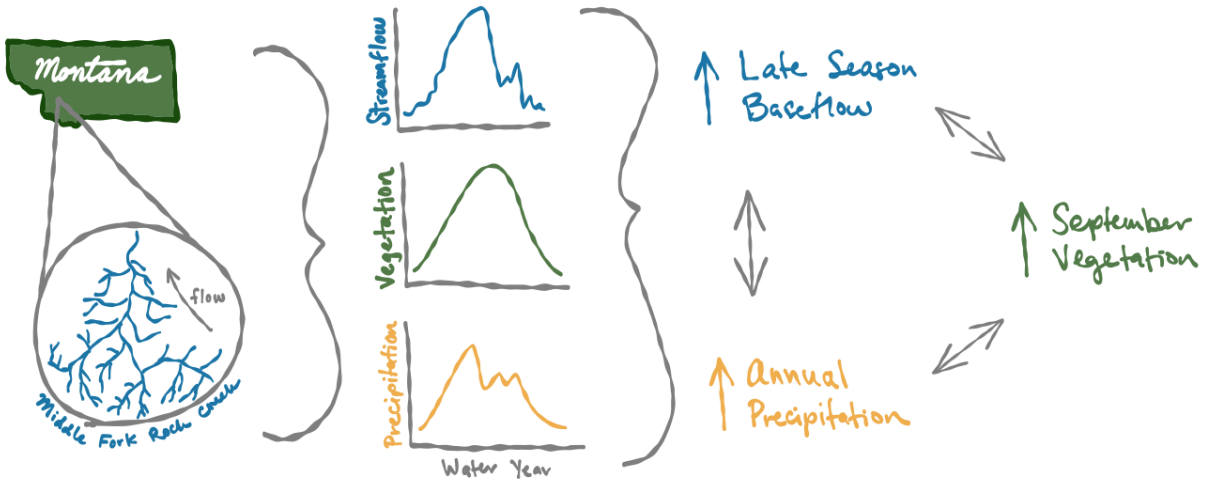

Keywords: water availability, hydrology, vegetation, precipitation, baseflow, Montana, MRRMaid

1. Introduction

With the effects of climate change already being felt (e.g. snow droughts (Huning and AghaKouchak, 2020) and megafires (Nolan et al., 2022)), changes in the timing and amount of precipitation, snowpack, and baseflows and their relation to water availability have become active areas of research. Water availability is generally decreasing in the western U.S. (Zhang et al., 2023), and a clear place to focus on monitoring it would be where all rivers begin – the headwaters. Headwater streams make up 77% of total stream length in and drain more than 73% of the coterminous U.S. (Strahler orders 1 and 2) (Lane et al., 2026), but they can be challenging to measure in the field because of their abundance. Satellite remote sensing with broad spatial and long temporal scales can help alleviate the time and resource burdens of field measurements, and have been used to detect surface water in many ways, as reviewed by Huang et al. (2018). At the scales of small streams regardless of their Strahler order, however, there are no publicly available, broad coverage, high spatial and temporal resolution (<10 m, and at least monthly) remote sensing datasets than can be used to directly measure surface water area (Huang et al., 2018), especially during baseflow when surface water area is at its smallest. Even if there was a free high-resolution product, it probably still would not be possible to measure the extent of these streams because of overhanging vegetation and other obstacles that obscure the water from above.

So how can water availability of these systems be measured efficiently? In the semi-arid Intermountain West of the U.S., there is a general feeling of "if it's green, it's wet" – especially in the summer. It follows that measures of vegetation have been used as proxies for surface water availability (Donnelly et al., 2016; Kolarik et al., 2023; Shrestha et al., 2024), but their use has not been tested rigorously against streamflow data. It is intuitive that vegetation presence and expanse would be a good proxy for surface water availability because flow regimes and vegetation are innately related (Merritt et al., 2010). Riparian vegetation function is acutely sensitive to changes in the flow regime (e.g. photosynthesis and carbon dioxide flux) and its characteristics reflect long-term changes in the flow regime (e.g. shoot/root growth, population growth rate, community richness, and stand biomass) (Merritt et al., 2010). Indeed, vegetation greening and water availability may be positively related in the Northern Hemisphere, where greening could be driving and/or responding to water availability (Zhang et al., 2023).

Baseflow periods are of particular interest because they sustain ecosystems during dry periods, and baseflow droughts are getting more severe (Lee and Ajami, 2023). Although some research has found that near-stream vegetation competes for and therefore can diminish flow during dry periods (Warix et al., 2023), it is possible that vegetation can be used as an indicator of overall catchment wetness and water availability for both evapotranspiration and streamflow (Bergstrom et al., 2025). The persistence of this relationship across ecoregions, the strength across disturbance regimes, and the temporal scales of vegetation-water availability coupling have yet to be tested. We aim to help fill this knowledge gap by providing additional evidence of coupling at both the decadal and intra-annual timescales in a relatively un-studied watershed.

Generally, it has gotten much easier to map vegetation across the four decades of available NASA Landsat imagery with the Google Earth Engine-based Mesic Resource Monitoring Aid Toolbox (MRRMaid) (Boise State University, 2025). MRRMaid provides inter- and intra-annual

estimates of floodplain vegetation coverage since 1984 across the sagebrush biome. These long time-series of floodplain vegetation can be used to assess the interconnectedness of climate, streamflow, and vegetation that are relevant in the context of changing hydrologic regimes due to climate change (Kundzewicz, 2008). This study provides additional evidence that remote sensing of vegetation is a way to monitor ecosystem health and response to climate change, in addition to possibly being a proxy for surface water availability.

1.1. Objectives

This study was conducted in the relatively unaltered Middle Fork Rock Creek watershed in southwestern Montana that has an active USGS gaging station with decades of streamflow measurements. This is an ideal place to rigorously test if floodplain vegetation presence and persistence is indicative of water availability in the late season and the semi-arid west. Specifically, our objectives are to determine (1) how climate, streamflow, and vegetation are trending (1984-2024) and (2) if and how strongly precipitation, late season baseflow, and September vegetation are correlated to each other.

2. Middle Fork Rock Creek

The Middle Fork Rock Creek watershed upstream of the USGS gage (#12332000) has a drainage area of 314 km^2, mean elevation of 2,174 m, mean annual precipitation of 75 cm, and mean annual temperature of 2.2°C (U.S. Geological Survey, 2025a) (Figure 1). The USGS Middle Fork Rock Creek gage is classified as a reference gage in the GAGESII dataset, meaning that it is a watershed with the lowest level of disturbance (Falcone, 2011). This makes it a natural laboratory to study the relationships between climate, streamflow, and vegetation without the direct added influence of humans. The watershed is mostly roadless with minor local water diversions and has never had dams (Falcone, 2011). There was no medium or high intensity development in the watershed in 1985 or in 2023 (Multi-Resolution Land Characteristics Consortium, 2025, vols. 1985 and 2023), but there is a history of cattle ranching, timber harvest, and recreational fishing and camping in the watershed (Berwick, 1968; Carnefix, 2002). There is one mining district in the watershed that did not seem to have been economically significant and so we infer not environmentally significant (Pederson, 1976; Loen and Pearson, 1984; U.S. Geological Survey, 2005; Ralph et al., 2025). The largest documented fire in the watershed since 1878 was the Meyers Fire in 2017 that burned most of the upper half of the watershed (Welty and Jeffries, 2020; National Interagency Fire Center, 2025). There is no published information regarding historical or current abundance or persistence of beaver populations in the watershed, but it falls squarely within their native range (Baker and Hill, 2003) and there is visual evidence on the ArcGIS Pro basemap imagery of some beaver activity (mainly dams) (Figure 1 inset).

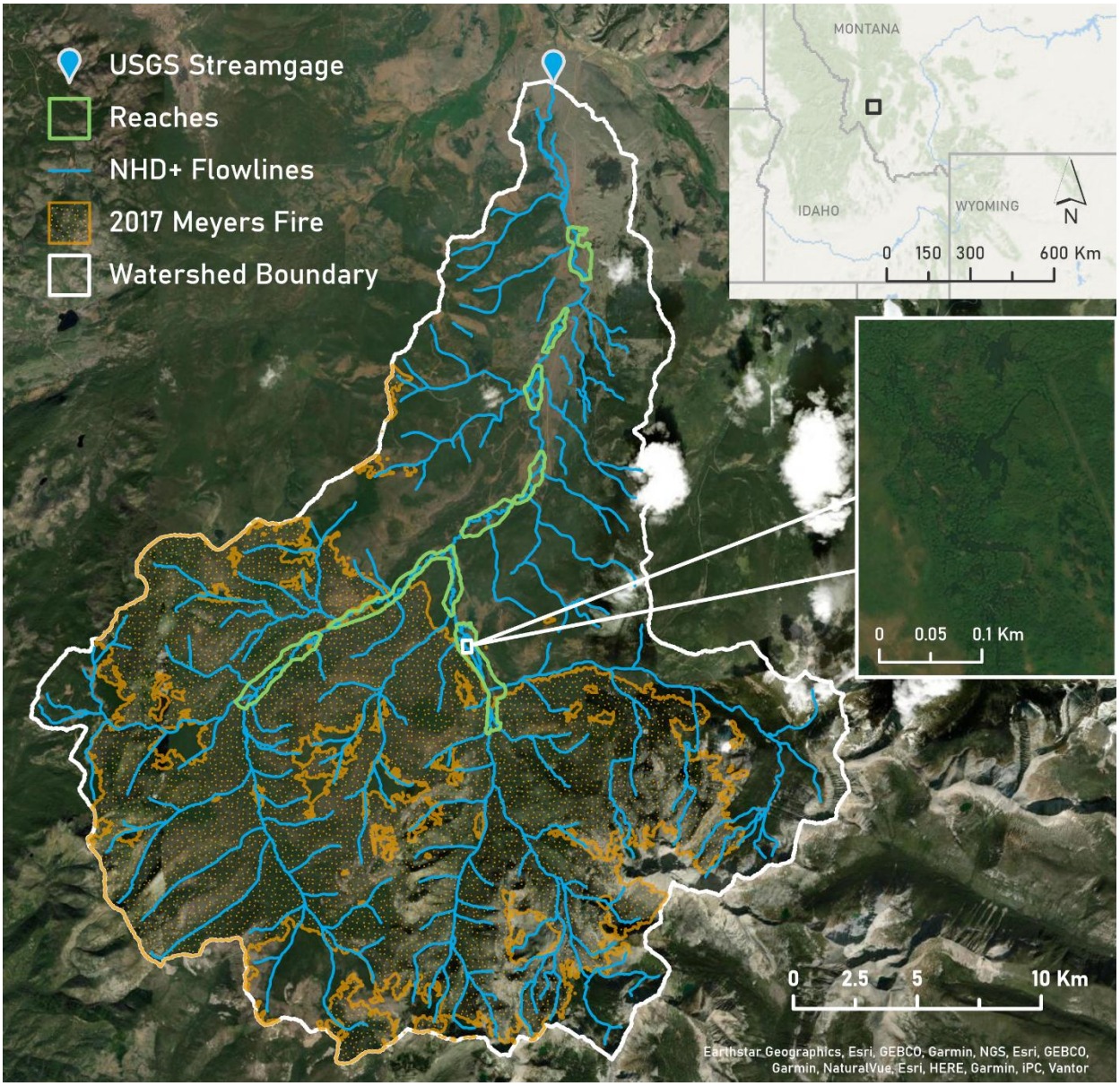

Figure 1. Middle Fork Rock Creek watershed in southwestern Montana, USA with broader location and beaver activity insets. The orange stippled area indicates the extent of the 2017 Meyers Fire.

The mainstems of Middle Fork Rock Creek and Copper Creek (its major western tributary) were split into eight geomorphic reaches that represent the majority of the wide low-gradient floodplains, or "beads", in the watershed (Figure 1). We assume that these eight reaches adequately represent floodplain conditions in the watershed (Wohl, 2021; Wohl et al., 2021), and took this approach to ensure vegetation was only mapped in floodplain areas (not hillslopes) and across the watershed without also needing high-powered computing. Going forward, "Middle Fork Rock Creek" refers to both streams as one. Note that the Meyers Fire perimeter does include portions of the upper three reaches.

3. Methods

The watershed boundary was delineated in StreamStats (U.S. Geological Survey, 2025a), and the eight geomorphic reaches previously described were delineated by hand in ArcGIS Pro (Esri, 2025) by modifying the Valley Bottom Extraction Tool polygon (Gilbert et al., 2016) for the watershed (Cybercastor, 2023) using 1-m resolution lidar-derived bare earth topography (from 2019-2020) (U.S. Geological Survey, 2022a, 2022b, 2022c, 2022b, 2022d, 2022e, 2022f, 2022g, 2022h), the derived hillshade raster, and basemap imagery (from April 2024).

We used the Mesic Vegetation Persistence (MVP) product from a modified version (Iskin et al., In Revision) of the MVPRestore (Rojas Lucero et al., 2024) Google Earth Engine (Gorelick et al., 2017) app to map vegetation through time across the eight reaches. This time series dataset consists of a point for each quality Landsat image (1984-2024) that represents the percentage of the reach that is classified as floodplain vegetation. This classification is based on user-defined thresholds of the Modified Chlorophyll Absorption Ratio Index (MCARI) and the Moisture Change Index (MCI) (Shrestha et al., 2024). The default index values were used (MCARI = 0.2 and MCI = 0.4) and the dates for each year were set to June 1 to September 30 to limit the analysis to the growing season and decrease the amount of missing data (Iskin et al., In Revision). The modified version of MVPRestore allows for direct polygon upload and decreases the cloud filter down from 20% to 50% to increase the number of data points used in the analysis (Iskin et al., In Revision). Visual inspection of the 2018-2024 10-m cover of Invasive Annual Grass dataset shows low values (<5% cover by reach) of invasive grasses across all eight reaches (Allred et al., 2025), indicating that there is high likelihood native riparian vegetation is being captured.

3.1. Streamflow, Vegetation, and Climate Metrics

The rest of the analysis was completed in R (R Core Team, 2025) using the *tidyverse* package (Wickham et al., 2019) with coding assistance from ChatGPT. All analyses were done on a water year basis (using October 1 as Water Year Day 1). Starting with the hydrologic data, we used the *dataRetrieval* R package (DeCicco et al., 2025) to pull daily total discharge data from October 1, 1983 to September 30, 2024 for the Middle Fork Rock Creek gage (U.S. Geological Survey, 2025b) (Figure S1). Discharge data were missing for November 1, 2006 to March 31, 2007 and for July 21, 2021 to July 22, 2021. Daily baseflow discharge was calculated (Figure S1), high flow periods were identified from the daily total discharge time series using the *hydrostats* package (Bond, 2022), and calculated the day of the water year that each high flow period started (# day) was calculated. Baseflow discharge (cfs) was calculated as a proportion of total discharge using $\alpha = 0.970$ ($\alpha_{default} = 0.975$) to get the baseflow hydrograph to more closely follow the total discharge on the falling limb (Figure S1). To identify high flow periods, a threshold value of 103 cfs (the upper quartile value for April of all years combined) was used and high flow values that were within 30 days of each other were combined (Figure S2). Lastly, water year flow volumes (AF) were calculated from (1) daily total discharge and (2) daily baseflow discharge for just August and September ("late season") of each year using the trapezoidal area-under-the-curve ("AUC") function from the *DescTools* package (Signorell, 2025). Going forward these variables are referred to simply as "high flow duration", "high flow start", "total volume", and "baseflow volume".

As cross-reach comparisons of floodplain vegetation were not the focus of this study, the reach-level vegetation data was combined into watershed-level data by taking the median of the

monthly values across reaches (Figure S3). Gaps in the floodplain vegetation data (due to clouds) were filled (10 missing month-years) by taking the average of the two previous and two following years' values for the same month, where available (Iskin et al., In Revision). Floodplain vegetation data were missing in September 1984, June 1987, July 1990, June 1993, June 2010, all months of 2012, and June 2023. Going forward these variables are referred to simply as "June vegetation", "July vegetation", "August vegetation", and "September vegetation".

DAYMET 1-km daily climate time series data (water years 1984-2024) (Thornton et al., 2022) downloaded from Climate Engine (Huntington et al., 2017; Desert Research Institute et al., 2025) as the climatic data. The gridded DAYMET time series are derived from interpolation, extrapolation, and statistical modeling of *in situ* climate data (Thornton et al., 1997; Thornton and Running, 1999; Thornton et al., 2000, 2021). We followed common practice and averaged climatic variables over the entire drainage basin (Newman et al., 2015; Li et al., 2025). We extracted watershed-average values of water year total daily precipitation (mm), water year maximum daily snow-water equivalent (SWE) (mm), and water year average daily average temperature (°C) (Figure S4). Going forward we will refer to these variables simply as "precipitation", "SWE", and "temperature".

3.2. Statistical Methods

The final data table used in the statistical analyses included for each water year: June, July, August, and September vegetation, high flow duration, high flow start, total volume, baseflow volume, precipitation, SWE, and temperature (Table S1). Correlation analyses are commonly used in hydrological studies (Yue et al., 2002; Kileshye Onema and Taigbenu, 2009; Wang et al., 2014; Moses et al., 2022). Following this, the non-parametric Spearman rank correlation values (ρ) for all variables were calculated and tested statistical significance using the *corrplot* R package (Wei and Simko, 2024) to assess the monotonic relationships between the variables (α = 0.05 for all tests). To assess the impact of trends through time on the correlations (Figures S5 and S6), we also took the first difference of each variable (Holmes et al., 2021; Righetti, 2025) (Table S2) and recalculated the correlations. Going forward the variables and correlations are referred to as either "observed" or "detrended". Auto- and cross-correlations were also calculated between September vegetation, baseflow volume, and precipitation because of the temporal variation of water availability. The data was lagged by one, two, and three water years (in both directions for cross-correlation), the resulting Spearman correlations were calculated, and statistical significance was tested.

4. Results

The following sections summarize the results of the various correlations analyses, including trends through time, relationships between observed variables, relationships between detrended variables, autocorrelation, and cross-correlation.

4.1. Trend analysis

There are many significant correlations among the ecologic, hydrologic, and climatic variables (Table 1 and Table 2). For the observed data, total volume (ρ = +0.35), SWE (ρ = -0.46), and temperature (ρ = +0.75) are all correlated with water year (Table 1), meaning that temperatures are rising, water available from snow is shrinking, but annual flow volumes are increasing. For

the detrended data, there are no statistically significant correlations with water year, indicating that the time series have been sufficiently detrended (Table 2).

4.2. Observed Relationships

For the observed time series (Table 1), greater precipitation is correlated with longer high flow durations (ρ = +0.55), larger total volumes (ρ = +0.70), and larger baseflow volumes to a greater extent (ρ = +0.76). Greater SWE is associated with longer high flow durations (ρ = +0.32) and larger total volumes (ρ = +0.32), but not larger baseflow volumes. Warmer temperatures are associated with smaller baseflow volumes (ρ = -0.39). A greater percentage of floodplain vegetation in August is associated with longer high flow durations (ρ = +0.33), larger total volumes (ρ = +0.40), and larger baseflow volumes to a greater extent (ρ = +0.53). Additionally, more September vegetation is correlated with longer high flow durations (ρ = +0.65), earlier start days of those high flows (ρ = -0.38), larger total volumes (ρ = +0.59), larger baseflow volumes (ρ = +0.54), more precipitation (ρ = +0.39), and greater SWE (ρ = +0.34). Note that precipitation and SWE do not appear to be strongly collinear (ρ = +0.34).

Table 1. Spearman rank correlations of the observed variables. Positive correlations are indicated in shades of blue and negative correlations are indicated in shades of orange, with darker colors indicating stronger monotonic relationships. Bold values indicate statistically significant correlations (α = 0.05).

	Water Year	June Vegetation	July Vegetation	Aug Vegetation	Sept Vegetation	High Flow Duration	High Flow Start	Total Volume	Baseflow Volume	Precipitation	SWE
June Vegetation	-0.04										
July Vegetation	0.14	-0.19									
Aug Vegetation	0.24	0.10	0.31								
Sept Vegetation	0.31	-0.13	**0.38**	**0.45**							
High Flow Duration	0.29	-0.12	0.17	**0.33**	**0.65**						
High Flow Start	-0.26	-0.01	-0.04	0.01	**-0.38**	**-0.57**					
Total Volume	**0.35**	-0.07	0.16	**0.40**	**0.59**	**0.74**	-0.27				
Baseflow Volume	0.12	-0.01	0.26	**0.53**	**0.54**	**0.70**	0.00	**0.74**			
Precipitation	-0.05	-0.02	0.09	0.25	**0.39**	**0.55**	0.04	**0.70**	**0.76**		
SWE	**-0.46**	0.01	0.13	0.03	**0.34**	**0.32**	-0.20	**0.32**	0.23	**0.34**	
Temperature	**0.75**	-0.06	-0.02	-0.05	-0.08	-0.04	-0.29	-0.04	**-0.39**	**-0.39**	**-0.53**

4.3. Detrended Relationships

For the detrended time series (Table 2), more precipitation is correlated with longer high flow durations (ρ = +0.69), larger total volumes (ρ = +0.85), and larger baseflow volumes (ρ = +0.83). Greater SWE is associated with longer high flow durations (ρ = +0.45) and larger total volumes (ρ = +0.50), but not larger baseflow volumes. Warmer temperatures are associated with earlier start days of high flows (ρ = -0.46) and smaller baseflow volumes (ρ = -0.55). A greater percentage of floodplain vegetation in June is associated with later start days of high flows (ρ = +0.32) and more July vegetation with larger baseflow volumes (ρ = +0.32). More August vegetation is correlated with larger total volumes (ρ = +0.32) and larger baseflow volumes (ρ = +0.44). Additionally, more September vegetation is correlated with longer high flow durations (ρ = +0.65), larger total volumes (ρ = +0.61), larger baseflow volumes (ρ = +0.58), more precipitation (ρ = +0.61), and cooler temperatures (ρ = -0.42).

Table 2. Spearman rank correlations of the detrended variables. Positive correlations are indicated in shades of blue and negative correlations are indicated in shades of orange, with darker colors indicating stronger monotonic relationships. Bold values indicate statistically significant correlations (α = 0.05).

	Water Year	June Vegetation	July Vegetation	Aug Vegetation	Sept Vegetation	High Flow Duration	High Flow Start	Total Volume	Baseflow Volume	Precipitation	SWE
June Vegetation	0.01										
July Vegetation	0.01	0.14									
Aug Vegetation	0.11	0.05	0.18								
Sept Vegetation	0.05	-0.07	0.08	0.30							
High Flow Duration	-0.05	-0.16	-0.05	0.20	**0.65**						
High Flow Start	0.03	**0.32**	0.28	0.21	-0.05	-0.27					
Total Volume	0.01	-0.16	0.15	**0.32**	**0.61**	**0.74**	0.01				
Baseflow Volume	0.05	0.07	**0.32**	**0.44**	**0.58**	**0.67**	**0.35**	**0.74**			
Precipitation	0.03	-0.05	0.11	0.25	**0.61**	**0.69**	0.18	**0.85**	**0.83**		
SWE	0.01	0.04	0.07	-0.02	0.29	**0.45**	-0.15	**0.50**	0.23	**0.31**	
Temperature	-0.04	-0.22	-0.16	-0.05	**-0.42**	-0.29	**-0.46**	-0.26	**-0.55**	**-0.48**	-0.09

4.4. Comparisons

Just looking at the climatic and hydrologic variables, almost all of the correlations strengthen when the detrended time series are used (Table 1 vs. Table 2). Notably, the correlations increased between temperature and high flow duration by 0.25, temperature and high flow start by 0.17, temperature and total volume by 0.22, and SWE and total volume by 0.18. Note that an increase in correlation strength could be in either the positive or negative direction. This indicates that interannual variation instead of long-term trends are driving the relationships between climate and flow. There is more variation in the change between September vegetation and the climatic and hydrologic variables when the detrended data are used. Most of the differences are $< \pm 0.05$, but there were three that were greater. The relationships between September vegetation and high flow start weakened by 0.33, precipitation strengthened by 0.22, and temperature strengthened by 0.34. The drop in strength between high flow start and September vegetation indicates that it was the opposite trends that were driving the relationship in the observed data and may not be a real interannual relationship.

If the correlations that are statistically significant for both the observed and detrended data that also stayed about the same or strengthened when using the detrended data are isolated, more September vegetation is associated with longer high flow durations, larger total volumes, larger baseflow volumes, and more precipitation. High flow duration, total volume, baseflow volume, and precipitation are also all reciprocally positively correlated with each other. Additionally, greater SWE is associated with longer high flow durations and larger total volumes, and higher temperatures are associated with lower baseflow volumes. Further isolating variables that (1) are derived from independent data sources, (2) represent late season river corridor conditions, and (3) are consistently significantly correlated, we can conclude that September vegetation, baseflow volume, and precipitation are all positively correlated.

4.1. Auto- and Cross-Correlations

Autocorrelations of the observed precipitation, baseflow volume, and September vegetation time series were calculated (Table 3). None of the variables appear to be strongly autocorrelated, but there is one statistically significant weak correlation between September vegetation and itself lagged one water year ($\rho = +0.33$). Cross-correlations of the same time series (Table 4) were calculated, and show that September vegetation does not lead or lag baseflow volume or

precipitation as is it only weakly cross-correlated with precipitation at a lag of -1 (ρ = -0.35), but not more so than at lag 0 (ρ = +0.39) (Table 1).

Table 3. Spearman rank autocorrelations of observed variables for lags of 1, 2, and 3 water years. Positive correlations are indicated in shades of blue and negative correlations are indicated in shades of orange, with darker colors indicating stronger monotonic relationships. Bold values indicate statistically significant correlations (α = 0.05).

	Lag 1	Lag 2	Lag 3
September Vegetation	**0.33**	0.23	0.23
Baseflow Volume	0.13	0.13	-0.09
Precipitation	0.01	-0.02	-0.17

Table 4. Spearman rank cross-correlations of observed variables for lags of -3, -2, -1, 1, 2, and 3 water years. Positive correlations are indicated in shades of blue and negative correlations are indicated in shades of orange, with darker colors indicating stronger monotonic relationships. Bold values indicate statistically significant correlations (α = 0.05) and bold bounding boxes indicate correlations that are significant and greater than the correlations between the same values at a lag of 0.

	Lag	**Baseflow Volume**	**Precipitation**
September Vegetation	*-3*	-0.13	-0.18
	-2	0.04	-0.12
	-1	-0.15	**-0.35**
	+1	0.25	0.19
	+2	0.06	0.01
	+3	0.11	-0.07

5. Discussion

Overall, the statistically significant 40-year trends of strongly increasing temperature and declining snowpack at the Middle Fork Rock Creek are consistent with what has been observed broadly across the western U.S. (Barnett et al., 2005; Mote et al., 2005; Pepin and Seidel, 2005; Knowles et al., 2006; Nayak et al., 2010; Pederson et al., 2011; Kapnick and Hall, 2012; McCabe et al., 2018). There isn't, however, an associated change in total precipitation, indicating that more precipitation is falling as rain instead of snow over time, which is supported by previous research (Knowles et al., 2006; Nayak et al., 2010; Abatzoglou, 2011). In southwestern Idaho, Nayak et al. (2010) found increasing temperatures, decreasing amounts of precipitation falling as snow, decreasing maximum SWE, but no changes in total precipitation or streamflow, whereas Luce and Holden (2009) found widespread decreases in streamflow across the Pacific Northwest. At the Middle Fork Rock Creek, total flow volume is increasing but precipitation, baseflow, and vegetation are not changing significantly. At first, this seems to indicate that more precipitation as rain in western Montana might be contributing more water to direct runoff instead of to aquifer recharge or evapotranspiration, but previous research shows that is it likely much more complicated than that (Hammond et al., 2019; Hammond and Kampf, 2020). The fate of precipitation depends on soil properties and depths (Hammond et al., 2019) and streamflow generation depends on both the form of precipitation and the seasonal timing of when it falls (Hammond and Kampf, 2020). Intra-annual analysis of precipitation, temperature, snowpack, and streamflow would be required to thoroughly understand what is occurring in this watershed, as suggested by the minimal decreases in runoff and mixed trends in runoff efficiency observed by McCabe et al. (2018) across the west.

Although the Middle Fork Rock Creek watershed is experiencing rising temperatures and decreasing SWE, it is not also experiencing the earlier peak flows that Colorado (Clow, 2010)

and the west generally (Stewart et al., 2005; McCabe et al., 2018) are experiencing. There aren't any strong and/or consistent correlations between early season vegetation and the hydroclimatic variables, but there is an increase in strength between baseflow and vegetation as the season progresses from August through September for both the observed and detrended data (and July for the detrended data). This could be because the measure of baseflow only includes August and September flow values in order to capture late season dynamics. Alternatively, potential transitions from perennial to intermittent flow in the late season and/or changes in groundwater levels and variability could be driving these intra-annual patterns depending on the vegetation species present (e.g. in the arid Ariona Sonoran Desert (Stromberg et al., 2007)) (Steinberg et al., 2020).

Importantly, more September vegetation is correlated with more precipitation and higher late season baseflow volumes in the same water year for both the observed and detrended time series, indicating that this is a real interannual relationship and not just a product of similar 40-year trends. In other words, more water in a given year means more water for both streamflow and vegetation. This is observed even though the perimeter of the 2017 Meyers Fire overlaps portions of the upper three reaches. These upper reaches are where beaver activity is visible and might be increasing the resistance of the vegetation to burning (Fairfax and Whittle, 2020). These findings also likely support the findings of Bergstrom et al. (2025) that the stream and the vegetation might not be in direct competition for available water, and improves on previous studies (e.g. (Newcomb and Godsey, 2023; Warix et al., 2023; Bergstrom et al., 2025) because it looks specifically at floodplain vegetation at seasonal timescales. Higher baseflow is likely supporting alluvial aquifers and providing water to floodplain vegetation (Cadol et al., 2012; Lupon et al., 2018; Newcomb and Godsey, 2023). These results also indicate that floodplain vegetation is likely an appropriate proxy for late season baseflow in this watershed. In-depth study of the Middle Fork Rock Creek watershed would be required to parse out the relative influence of water sources to the study reaches in space and in time (i.e. upstream alluvial aquifers, deep groundwater, hillslope contributions), as the interplay of groundwater, streamflow, baseflow, and floodplain vegetation is complex and heterogeneous (Hughes, 1997; Mueller et al., 2013; Tan et al., 2025).

6. Conclusions

In the relatively undisturbed Middle Fork Rock Creek watershed, rising temperatures and declining snowpack but stable precipitation may not be having a negative effect on late season baseflow or floodplain vegetation. In the same water year, higher baseflow volumes are associated with greater coverage of floodplain vegetation and more precipitation. If more precipitation is falling as rain and contributing directly to total flow, then adaptation and restoration efforts may want to focus on natural forms of water storage up in the headwaters, such as beaver complexes and naturally-functioning floodplains, to help recharge aquifers and attenuate disturbances (e.g. floods, fires, debris flows) in the event that the total amount, seasonality, or intensity of precipitation does significantly change. This study also demonstrates an accessible way to monitor late-season baseflow by measuring September vegetation using remote sensing in ungaged watersheds. More study is needed to determine how these relationships might relate to stream drying; how they might vary across snow-dominated watersheds of varying size, topography, and ecoregion; and how they might differ for human-altered watersheds. Future studies could make use of the entire dataset of GAGESII reference

watersheds to investigate these trends and further determine if floodplain vegetation is an appropriate proxy for surface water availability generally across the U.S.

CRediT Author Statement

E. Iskin: Conceptualization, Methodology, Software, Formal Analysis, Investigation, Data Curation, Writing - Original Draft, Writing - Review and Editing, Visualization, Project Administration. **A. Bergstrom**: Conceptualization, Methodology, Validation, Writing - Review and Editing. **J. Brandt**: Conceptualization, Resources, Writing - Review and Editing, Supervision, Funding Acquisition.

Acknowledgements

This work was supported by the National Aeronautics and Space Administration (NASA) [grant numbers 80NSSC25K7236, 80NSSC21K1624] and the U.S. Department of Agriculture (USDA) National Institute of Food and Agriculture (NIFA) [grant number 2022-11619]. The authors would like to thank Juan Camilo Rojas Lucero (Boise State University) for assistance with the modified version of the MVPRestore app used in this study to obtain the vegetation time series, and Ann Hess (Colorado State University) and Trevor Caughlin (Boise State University) for providing input on the statistical analysis.

Data statement

The floodplain vegetation data used in the study are publicly available from the MVPRestore Google Earth Engine app that is linked on this homepage: https://www.boisestate.edu/hes/projects/mrrmaid-mesic-resource-restoration-monitoring-aid/. The climate data are available from the Climate Engine App via https://app.climateengine.org/, and the discharge data are available from the U.S. Geological Survey's Water Data for the Nation website via https://waterdata.usgs.gov/. The elevation data can be accessed through The National Map downloader tool via https://apps.nationalmap.gov/downloader/ and the VBET data are available from the Riverscapes Data Exchange via https://data.riverscapes.net/. Shapefiles of the delineated watershed and floodplain reaches will be shared upon request.

References

Abatzoglou, J.T., 2011. Influence of the PNA on declining mountain snowpack in the Western United States. Int. J. Climatol. 31, 1135–1142. https://doi.org/10.1002/joc.2137

Allred, B.W., McCord, S.E., Assal, T.J., Bestelmeyer, B.T., Boyd, C.S., Brooks, A.C., Cady, S.M., Fuhlendorf, S.D., Green, S.A., Harrison, G.R., Jensen, E.R., Kachergis, E.J., Mattilio, C.M., Mealor, B.A., Naugle, D.E., O'Leary, D., Olsoy, P.J., Peirce, E.S., Reinhardt, J.R., Shriver, R.K., Smith, J.T., Tack, J.D., Tanner, A.M., Tanner, E.P., Twidwell, D., Webb, N.P., Morford, S.L., 2025. Sentinel-2 based estimates of rangeland fractional cover and canopy gap class for the western United States. https://doi.org/10.1101/2025.03.13.643073

Baker, B.W., Hill, E.P., 2003. Beaver (Castor canadensis), in: Feldhamer, G.A., Thompson, B.C., Chapman, J.A. (Eds.), Wild Mammals of North America: Biology, Management, and Conservation. The Johns Hopkins University Press, Baltimore, MD, pp. 288–310.

Barnett, T.P., Adam, J.C., Lettenmaier, D.P., 2005. Potential impacts of a warming climate on water availability in snow-dominated regions. Nature 438, 303–309. https://doi.org/10.1038/nature04141

Bergstrom, A., Price, A.N., Beers, M., Roche, K.R., 2025. Climate Forcings Across Multiple Timescales Control Stream Drying and Wetting in a Headwater Catchment. Hydrol. Process. 39, e70167. https://doi.org/10.1002/hyp.70167

Berwick, S.H., 1968. Observations on the decline of the Rock Creek Montana population of bighorn sheep (Master of Science). University of Montana, Missoula, MT.

Boise State University, 2025. MRRMaid: Mesic Resource Restoration Monitoring Aid [WWW Document]. Hum.-Environ. Syst. URL https://www.boisestate.edu/hes/projects/mrrmaid-mesic-resource-restoration-monitoring-aid/

Bond, N., 2022. hydrostats: Hydrologic Indices for Daily Time Series Data.

Cadol, D., Kampf, S., Wohl, E., 2012. Effects of evapotranspiration on baseflow in a tropical headwater catchment. J. Hydrol., Tropical Hydrology 462–463, 4–14. https://doi.org/10.1016/j.jhydrol.2012.04.060

Carnefix, G., 2002. Movement patterns of fluvial bull trout in relation to habitat parameters in the Rock Creek drainage Missoula and Granite Counties Montana (Master of Science). University of Montana, Missoula, MT.

Clow, D.W., 2010. Changes in the Timing of Snowmelt and Streamflow in Colorado: A Response to Recent Warming. https://doi.org/10.1175/2009JCLI2951.1

Cybercastor, 2023. Valley Bottom for Middle Fork Rock Creek.

DeCicco, L., Hirsch, R., Lorenz, D., Watkins, D., Blodgett, D., Johnson, M., 2025. dataRetrieval: R packages for discovering and retrieving water data available from U.S. Federal hydrologic web services. https://doi.org/10.5066/P9X4L3GE

Desert Research Institute, University of California, Merced, Google, NOAA National Integrated Drought Information System, Bureau of Land Management, 2025. ClimateEngine.org [WWW Document]. URL https://app.climateengine.org/climateEngine

Donnelly, J.P., Naugle, D.E., Hagen, C.A., Maestas, J.D., 2016. Public lands and private waters: scarce mesic resources structure land tenure and sage-grouse distributions. Ecosphere 7, e01208. https://doi.org/10.1002/ecs2.1208

Esri, 2025. ArcGIS Pro.

Fairfax, E., Whittle, A., 2020. Smokey the Beaver: beaver-dammed riparian corridors stay green during wildfire throughout the western United States. Ecol. Appl. 30, e02225. https://doi.org/10.1002/eap.2225

Falcone, J., 2011. GAGES-II: Geospatial Attributes of Gages for Evaluating Streamflow. https://doi.org/10.5066/P96CPHOT

Gilbert, J.T., Macfarlane, W.W., Wheaton, J.M., 2016. The Valley Bottom Extraction Tool (V-BET): A GIS tool for delineating valley bottoms across entire drainage networks. Comput. Geosci. 97, 1–14. https://doi.org/10.1016/j.cageo.2016.07.014

Gorelick, N., Hancher, M., Dixon, M., Ilyushchenko, S., Thau, D., Moore, R., 2017. Google Earth Engine: Planetary-scale geospatial analysis for everyone. Remote Sens. Environ. 202, 18–27. https://doi.org/10.1016/j.rse.2017.06.031

Hammond, J.C., Harpold, A.A., Weiss, S., Kampf, S.K., 2019. Partitioning snowmelt and rainfall in the critical zone: effects of climate type and soil properties. Hydrol. Earth Syst. Sci. 23, 3553–3570. https://doi.org/10.5194/hess-23-3553-2019

Hammond, J.C., Kampf, S.K., 2020. Subannual Streamflow Responses to Rainfall and Snowmelt Inputs in Snow-Dominated Watersheds of the Western United States. Water Resour. Res. 56, e2019WR026132. https://doi.org/10.1029/2019WR026132

Holmes, E.E., Scheuerell, M.D., Ward, E.J., 2021. Applied time series analysis for fisheries and environmental data. University of Washington.

Huang, C., Chen, Y., Zhang, S., Wu, J., 2018. Detecting, Extracting, and Monitoring Surface Water From Space Using Optical Sensors: A Review. Rev. Geophys. 56, 333–360. https://doi.org/10.1029/2018RG000598

Hughes, F.M.R., 1997. Floodplain biogeomorphology. Prog. Phys. Geogr. Earth Environ. 21, 501–529. https://doi.org/10.1177/030913339702100402

Huning, L.S., AghaKouchak, A., 2020. Global snow drought hot spots and characteristics. Proc. Natl. Acad. Sci. 117, 19753–19759. https://doi.org/10.1073/pnas.1915921117

Huntington, J.L., Hegewisch, K.C., Daudert, B., Morton, C.G., Abatzoglou, J.T., McEvoy, D.J., Erickson, T., 2017. Climate Engine: Cloud Computing and Visualization of Climate and Remote Sensing Data for Advanced Natural Resource Monitoring and Process Understanding. Bull. Am. Meteorol. Soc. 98, 2397–2410. https://doi.org/10.1175/BAMS-D-15-00324.1

Iskin, E., Kolarik, N., Rojas Lucero, J.C., Brandt, J., In Revision. Monitoring Change in Floodplain Vegetation due to River Restoration Treatments with Remote Sensing in the Intermountain West. Water Resour. Res.

Kapnick, S., Hall, A., 2012. Causes of recent changes in western North American snowpack. Clim. Dyn. 38, 1885–1899. https://doi.org/10.1007/s00382-011-1089-y

Kileshye Onema, J.-M., Taigbenu, A., 2009. NDVI–rainfall relationship in the Semliki watershed of the equatorial Nile. Phys. Chem. Earth Parts ABC, 9th WaterNet/WARFSA/GWP-SA Symposium: Water and Sustainable Development for Improved Livelihoods 34, 711–721. https://doi.org/10.1016/j.pce.2009.06.004

Knowles, N., Dettinger, M.D., Cayan, D.R., 2006. Trends in Snowfall versus Rainfall in the Western United States. J Climate. https://doi.org/10.1175/JCLI3850.1

Kolarik, N., Roopsind, A., Pickens, A., Brandt, J., 2023. A satellite-based monitoring system for quantifying surface water and mesic vegetation dynamics in a semi-arid region. Ecol. Indic. 147, 109965. https://doi.org/10.1016/j.ecolind.2023.109965

Kundzewicz, Z.W., 2008. Climate change impacts on the hydrological cycle. Ecohydrol. Hydrobiol. 8, 195–203. https://doi.org/10.2478/v10104-009-0015-y

Lane, C.R., D'Amico, E., Christensen, J.R., Golden, H.E., Cheng, F.Y., Hammond, J.C., Husic, A., Jaeger, K.L., Jones, C.N., Kelleher, C.A., Li, L., Mahoney, D.T., McMillan, H.K., Price, A.N., Sando, R., Segura, C., Seybold, E.C., Ward, A.S., Zimmer, M., 2026. Identifying Headwater Streams across the Conterminous United States. Ecosystems 29, 22. https://doi.org/10.1007/s10021-025-01041-z

Lee, S., Ajami, H., 2023. Comprehensive assessment of baseflow responses to long-term meteorological droughts across the United States. J. Hydrol. 626, 130256. https://doi.org/10.1016/j.jhydrol.2023.130256

Li, J., Hsu, K., Sorooshian, S., Lu, D., 2025. From Lumped to Spatially Distributed Hydrologic Models: A Generalizable Data-Driven Framework Across North America. https://doi.org/10.22541/essoar.176556008.89599411/v1

Loen, J.S., Pearson, R.C., 1984. Mines and propects in the Dillon 1° x 2° quadrangle, Idaho and Montana (Open-File Report No. 84–377). U.S. Geological Survey, Denver, CO.

Luce, C.H., Holden, Z.A., 2009. Declining annual streamflow distributions in the Pacific Northwest United States, 1948–2006. Geophys. Res. Lett. 36. https://doi.org/10.1029/2009GL039407

Lupon, A., Ledesma, J.L.J., Bernal, S., 2018. Riparian evapotranspiration is essential to simulate streamflow dynamics and water budgets in a Mediterranean catchment. Hydrol. Earth Syst. Sci. 22, 4033–4045. https://doi.org/10.5194/hess-22-4033-2018

McCabe, G.J., Wolock, D.M., Valentin, M., 2018. Warming is Driving Decreases in Snow Fractions While Runoff Efficiency Remains Mostly Unchanged in Snow-Covered Areas of the Western United States. https://doi.org/10.1175/JHM-D-17-0227.1

Merritt, D.M., Scott, M.L., Poff, N.L., Auble, G.T., Lytle, D.A., 2010. Theory, methods and tools for determining environmental flows for riparian vegetation: riparian vegetation-flow response guilds. Freshw. Biol. 55, 206–225. https://doi.org/10.1111/j.1365-2427.2009.02206.x

Moses, O., Blamey, R.C., Reason, C.J.C., 2022. Relationships between NDVI, river discharge and climate in the Okavango River Basin region. Int. J. Climatol. 42, 691–713. https://doi.org/10.1002/joc.7267

Mote, P.W., Hamlet, A.F., Clark, M.P., Lettenmaier, D.P., 2005. Declining Mountain Snowpack in Western North America. https://doi.org/10.1175/BAMS-86-1-39

Mueller, M.H., Weingartner, R., Alewell, C., 2013. Importance of vegetation, topography and flow paths for water transit times of base flow in alpine headwater catchments. Hydrol. Earth Syst. Sci. 17, 1661–1679. https://doi.org/10.5194/hess-17-1661-2013

Multi-Resolution Land Characteristics Consortium, 2025. Annual NLCD Land Cover (CONUS).

National Interagency Fire Center, 2025. Interagency Fire Perimeter History (All Years View).

Nayak, A., Marks, D., Chandler, D.G., Seyfried, M., 2010. Long-term snow, climate, and streamflow trends at the Reynolds Creek Experimental Watershed, Owyhee Mountains, Idaho, United States. Water Resour. Res. 46. https://doi.org/10.1029/2008WR007525

Newcomb, S.K., Godsey, S.E., 2023. Nonlinear Riparian Interactions Drive Changes in Headwater Streamflow. Water Resour. Res. 59, e2023WR034870. https://doi.org/10.1029/2023WR034870

Newman, A.J., Clark, M.P., Sampson, K., Wood, A., Hay, L.E., Bock, A., Viger, R.J., Blodgett, D., Brekke, L., Arnold, J.R., Hopson, T., Duan, Q., 2015. Development of a large-sample watershed-scale hydrometeorological data set for the contiguous USA: data set characteristics and assessment of regional variability in hydrologic model performance. Hydrol. Earth Syst. Sci. 19, 209–223. https://doi.org/10.5194/hess-19-209-2015

Nolan, R.H., Anderson, L.O., Poulter, B., Varner, J.M., 2022. Increasing threat of wildfires: the year 2020 in perspective: A Global Ecology and Biogeography special issue. Glob. Ecol. Biogeogr. 31, 1898–1905. https://doi.org/10.1111/geb.13588

Pederson, G.T., Gray, S.T., Woodhouse, C.A., Betancourt, J.L., Fagre, D.B., Littell, J.S., Watson, E., Luckman, B.H., Graumlich, L.J., 2011. The Unusual Nature of Recent Snowpack Declines in the North American Cordillera. Science 333, 332–335. https://doi.org/10.1126/science.1201570

Pederson, R.J., 1976. Geology of the Upper Rock Creek Drainage, Granite County, Montana (Master of Science). Montana College of Mineral Science and Technology, Butte, MT.

Pepin, N.C., Seidel, D.J., 2005. A global comparison of surface and free-air temperatures at high elevations. J. Geophys. Res. Atmospheres 110. https://doi.org/10.1029/2004JD005047

R Core Team, 2025. R: A language and environment for statistical computing.

Ralph, J., Von Bargen, D., Martynov, P., Zhang, J., Que, X., Prabhu, A., Morrison, S.M., Li, W., Chen, W., Ma, X., 2025. Mindat.org: The open access mineralogy database to accelerate data-intensive geoscience research. Am. Mineral. 110, 833–844. https://doi.org/10.2138/am-2024-9486

Righetti, N., 2025. Time Series Analysis With R. University of Vienna.

Rojas Lucero, J.C., Iskin, E., Shrestha, N., Kolarik, N., Brandt, J., 2024. Decision Support Tool – GEE Web App for MRRMaid MVPRestore. MRRMaid Toolbox.

Shrestha, N., Kolarik, N., Brandt, J., 2024. Mesic vegetation persistence: A new approach for monitoring spatial and temporal changes in water availability in dryland regions using cloud computing and the sentinel and Landsat constellations. Sci. Total Environ. 917, 170491. https://doi.org/10.1016/j.scitotenv.2024.170491

Signorell, A., 2025. DescTools: Tools for Descriptive Statistics.

Steinberg, K.A., Eichhorst, K.D., Rudgers, J.A., 2020. Riparian plant species differ in sensitivity to both the mean and variance in groundwater stores. J. Plant Ecol. 13, 621–632. https://doi.org/10.1093/jpe/rtaa049

Stewart, I.T., Cayan, D.R., Dettinger, M.D., 2005. Changes toward Earlier Streamflow Timing across Western North America. https://doi.org/10.1175/JCLI3321.1

Stromberg, J.C., Beauchamp, V.B., Dixon, M.D., Lite, S.J., Paradzick, C., 2007. Importance of low-flow and high-flow characteristics to restoration of riparian vegetation along rivers in arid south-western United States. Freshw. Biol. 52, 651–679. https://doi.org/10.1111/j.1365-2427.2006.01713.x

Tan, Xuejin, Tan, Xuezhi, Liu, B., Huang, Z., Fu, J., Peng, H., Zhang, W., 2025. Impacts of Anthropogenic Climate Change and Vegetation Variations on Global Changes in Baseflow and Stormflow. Water Resour. Res. 61, e2025WR040309. https://doi.org/10.1029/2025WR040309

Thornton, M.M., Shrestha, R., Wei, Y., Thornton, P.E., Kao, S.-C., 2022. Daymet: Daily Surface Weather Data on a 1-km Grid for North America, Version 4 R1. https://doi.org/10.3334/ORNLDAAC/2129

Thornton, P.E., Hasenauer, H., White, M.A., 2000. Simultaneous estimation of daily solar radiation and humidity from observed temperature and precipitation: an application over complex terrain in Austria. Agric. For. Meteorol. 104, 255–271. https://doi.org/10.1016/S0168-1923(00)00170-2

Thornton, P.E., Running, S.W., 1999. An improved algorithm for estimating incident daily solar radiation from measurements of temperature, humidity, and precipitation. Agric. For. Meteorol. 93, 211–228. https://doi.org/10.1016/S0168-1923(98)00126-9

Thornton, P.E., Running, S.W., White, M.A., 1997. Generating surfaces of daily meteorological variables over large regions of complex terrain. J. Hydrol., Aggregate Description of Land-Atmosphere Interactions 190, 214–251. https://doi.org/10.1016/S0022-1694(96)03128-9

Thornton, P.E., Shrestha, R., Thornton, M., Kao, S.-C., Wei, Y., Wilson, B.E., 2021. Gridded daily weather data for North America with comprehensive uncertainty quantification. Sci. Data 8, 190. https://doi.org/10.1038/s41597-021-00973-0

U.S. Geological Survey, 2025a. StreamStats.

U.S. Geological Survey, 2025b. Middle Fork Rock Cr nr Philipsburg MT - USGS-12332000.

U.S. Geological Survey, 2022a. USGS 1 Meter 12 x29y510 MT_RavalliGraniteCusterPowder_2019_B19.

U.S. Geological Survey, 2022b. USGS 1 Meter 12 x29y511 MT_RavalliGraniteCusterPowder_2019_B19.

U.S. Geological Survey, 2022c. USGS 1 Meter 12 x29y512 MT_RavalliGraniteCusterPowder_2019_B19.

U.S. Geological Survey, 2022d. USGS 1 Meter 12 x30y510 MT_RavalliGraniteCusterPowder_2019_B19.

U.S. Geological Survey, 2022e. USGS 1 Meter 12 x30y511 MT_RavalliGraniteCusterPowder_2019_B19.

U.S. Geological Survey, 2022f. USGS 1 Meter 12 x30y512 MT_RavalliGraniteCusterPowder_2019_B19.

U.S. Geological Survey, 2022g. USGS 1 Meter 12 x31y510 MT_RavalliGraniteCusterPowder_2019_B19.

U.S. Geological Survey, 2022h. USGS 1 Meter 12 x31y511 MT_RavalliGraniteCusterPowder_2019_B19.

U.S. Geological Survey, 2005. Mineral Resources Data System (MRDS).

Wang, F., Wang, X., Zhao, Y., Yang, Z., 2014. Correlation analysis of NDVI dynamics and hydro-meteorological variables in growth period for four land use types of a water scarce area. Earth Sci. Inform. 7, 187–196. https://doi.org/10.1007/s12145-013-0139-x

Warix, S.R., Godsey, S.E., Flerchinger, G., Havens, S., Lohse, K.A., Bottenberg, H.C., Chu, X., Hale, R.L., Seyfried, M., 2023. Evapotranspiration and groundwater inputs control the timing of diel cycling of stream drying during low-flow periods. Front. Water 5. https://doi.org/10.3389/frwa.2023.1279838

Wei, T., Simko, V., 2024. R package "corrplot": Visualization of a Correlation Matrix.

Welty, J.L., Jeffries, M.I., 2020. Combined wildfire datasets for the United States and certain territories, 1878-2019. https://doi.org/10.5066/P9Z2VVRT

Wickham, H., Averick, M., Bryan, J., Chang, W., McGowan, L.D., François, R., Grolemund, G., Hayes, A., Henry, L., Hester, J., Kuhn, M., Pedersen, T.L., Miller, E., Bache, S.M., Müller, K., Ooms, J., Robinson, D., Seidel, D.P., Spinu, V., Takahashi, K., Vaughan, D., Wilke, C., Woo, K., Yutani, H., 2019. Welcome to the tidyverse. J. Open Source Softw. 4, 1686. https://doi.org/10.21105/joss.01686

Wohl, E., 2021. An Integrative Conceptualization of Floodplain Storage. Rev. Geophys. 59, e2020RG000724. https://doi.org/10.1029/2020RG000724

Wohl, E., Castro, J., Cluer, B., Merritts, D., Powers, P., Staab, B., Thorne, C., 2021. Rediscovering, Reevaluating, and Restoring Lost River-Wetland Corridors. Front. Earth Sci. 9, 653623. https://doi.org/10.3389/feart.2021.653623

Yue, S., Pilon, P., Cavadias, G., 2002. Power of the Mann–Kendall and Spearman's rho tests for detecting monotonic trends in hydrological series. J. Hydrol. 259, 254–271. https://doi.org/10.1016/S0022-1694(01)00594-7

Zhang, Y., Li, C., Chiew, F.H.S., Post, D.A., Zhang, X., Ma, N., Tian, J., Kong, D., Leung, L.R., Yu, Q., Shi, J., Liu, C., 2023. Southern Hemisphere dominates recent decline in global water availability. Science 382, 579–584. https://doi.org/10.1126/science.adh0716

Supplemental Information

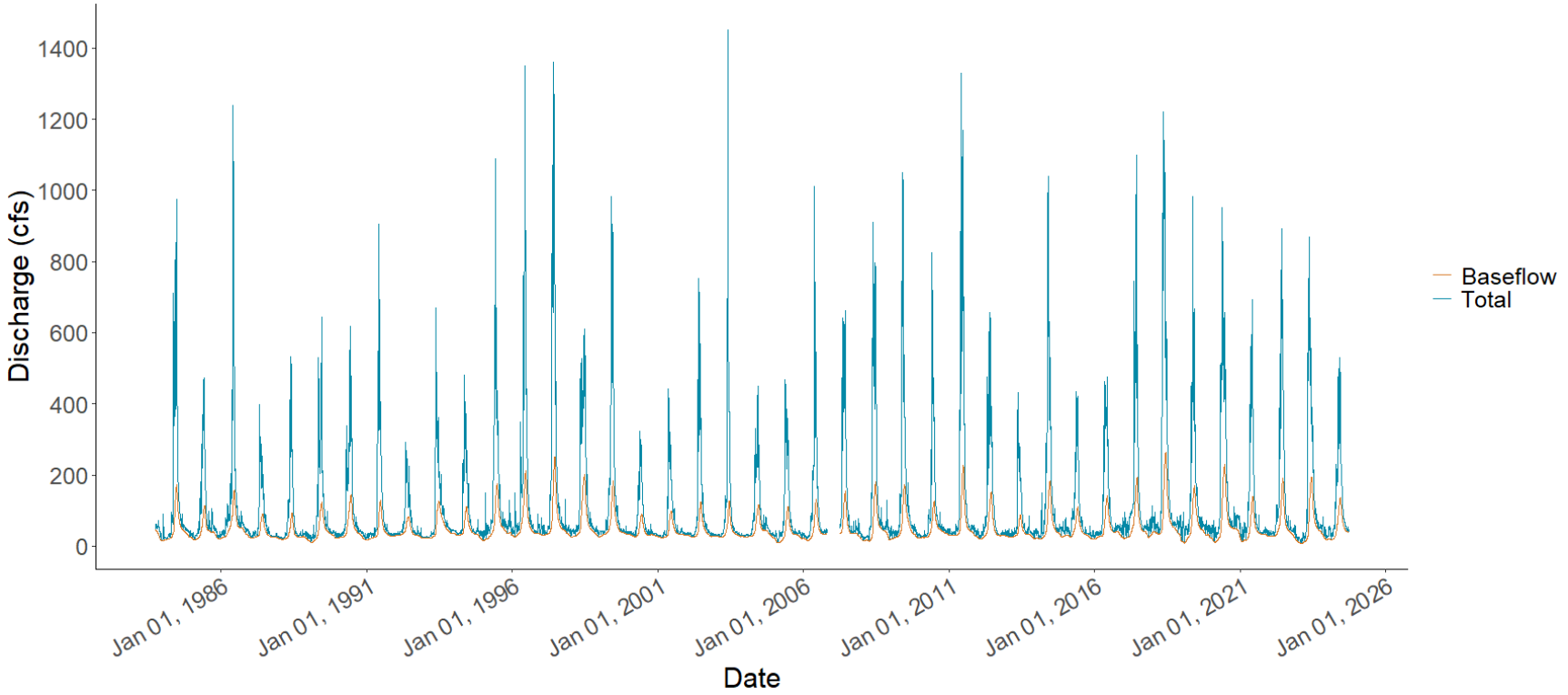

Figure S1. Daily total (blue) and baseflow (orange) discharge for Middle Fork Rock Creek, Montana (October 1, 1983-September 30, 2024).

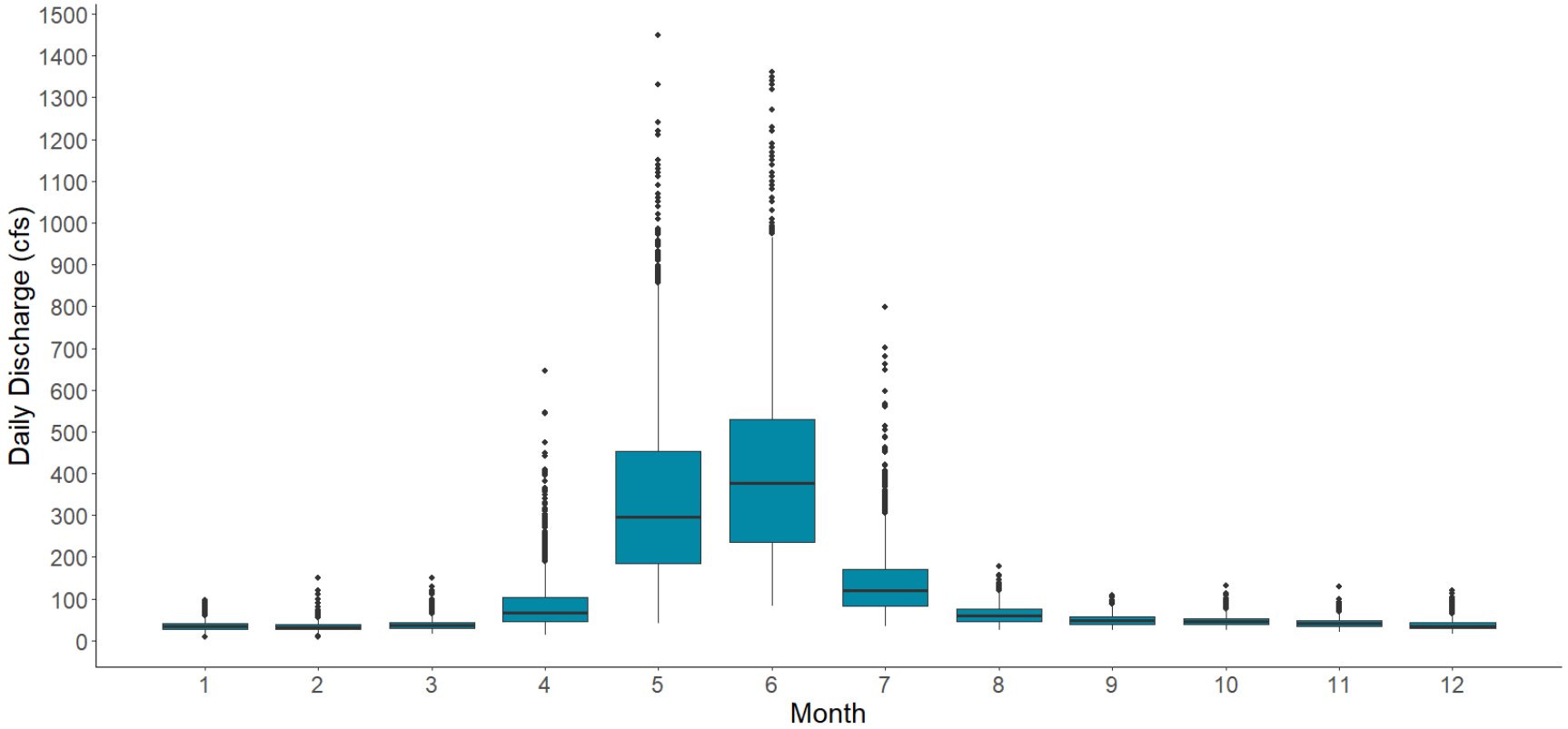

Figure S2. Monthly total discharge values for Middle Fork Rock Creek, Montana (1984-2024).

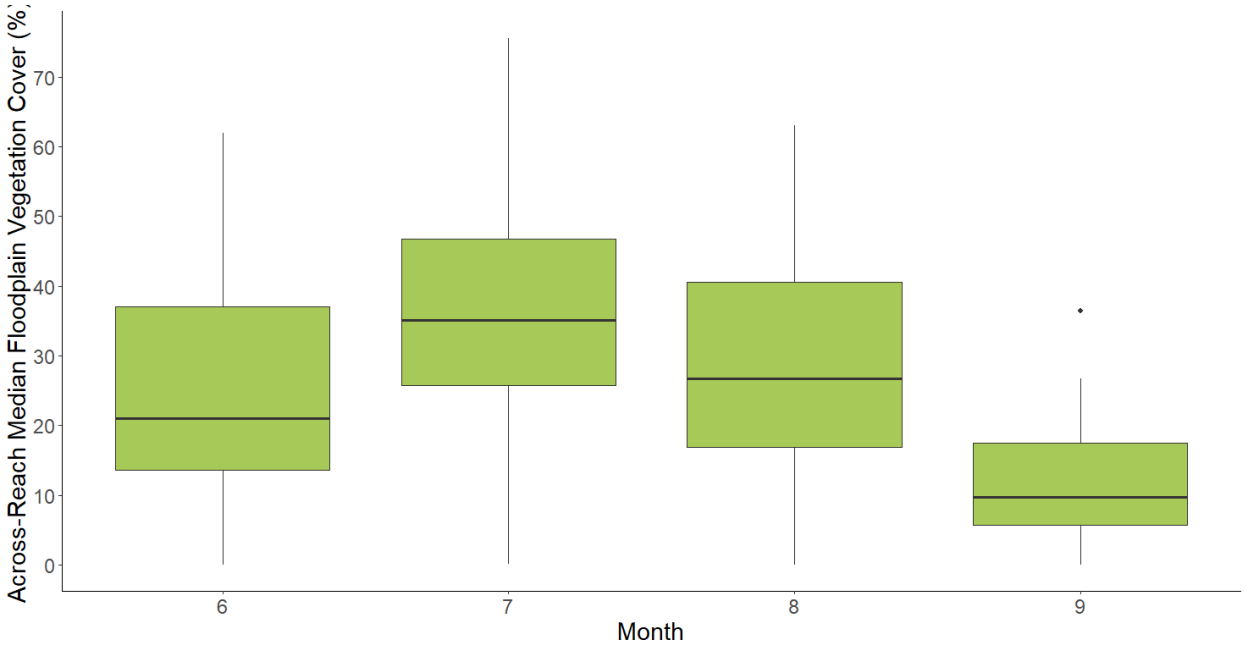

Figure S3. June, July, August, and September across-reach median floodplain vegetation values before gap-filling and outlier removal for Middle Fork Rock Creek, Montana (1984-2024).

Figure S4. DAYMET drainage area-averaged water year time series of daily: (a) total precipitation, (b) maximum snow-water equivalent, and (c) mean temperature for the Middle Fork Rock Creek, Montana (1984-2024).

Table S1. Complete gap-filled vegetation, hydrologic, and climatic data for the Middle Fork Rock Creek watershed, Montana by water year. For this table, vegetation and temperature values have been rounded to the nearest tenth, and flow duration, start day, volumes, precipitation, and snow-water equivalent to the nearest whole number.

Water Year	June Veg (%)	July Veg (%)	Aug Veg (%)	Sept Veg (%)	High Flow Duration (days)	High Flow Start (# day)	Total Volume (AF)	Baseflow Volume (AF)	Precipitation (mm)	SWE (mm)	Temperature (℃)
1984	62.0	37.0	47.0	17.8	84	225	91,247	5,975	821	331	0.4
1985	31.4	28.0	27.5	9.7	80	196	64,534	4,873	694	258	-0.3
1986	38.9	53.1	55.1	25.8	119	178	94,424	6,236	789	278	1.1
1987	35.5	41.9	25.8	2.3	62	206	52,460	3,483	553	220	2.7
1988	35.2	19.5	8.0	5.6	74	201	52,206	3,097	594	250	2.3
1989	36.7	49.4	3.3	6.6	94	202	64,516	5,024	739	274	2.0
1990	0.0	35.2	0.0	24.1	93	198	73,038	5,040	665	272	2.5
1991	9.8	29.5	17.6	20.5	73	227	71,212	4,693	663	244	1.7
1992	4.5	42.3	0.0	0.4	66	212	48,167	3,815	588	154	2.7
1993	14.6	32.5	35.4	11.0	109	223	69,504	7,552	832	164	0.4
1994	11.6	33.9	23.7	1.3	82	202	62,952	4,497	491	203	2.6
1995	32.4	22.3	31.3	6.3	96	218	93,511	6,657	804	177	1.4
1996	19.8	34.7	19.2	11.9	115	193	116,220	5,624	853	392	1.5
1997	0.0	38.2	39.7	10.6	121	202	132,505	6,927	950	231	1.8
1998	7.9	54.4	43.0	10.1	104	210	98,522	6,603	778	236	2.7
1999	45.3	25.1	1.4	12.6	115	202	100,001	5,917	695	187	2.1
2000	45.9	12.7	14.8	1.2	73	206	51,882	3,817	502	171	3.4
2001	19.1	0.2	10.8	2.2	94	211	54,471	4,499	544	168	2.7
2002	17.7	46.8	35.8	8.7	69	227	70,342	4,956	663	120	2.3
2003	17.1	26.8	19.7	0.0	80	205	74,088	4,190	686	225	3.5
2004	28.3	38.6	29.8	6.9	84	211	60,666	5,326	754	134	2.8
2005	54.5	37.9	29.2	2.8	69	220	59,411	4,222	576	143	3.1
2006	19.0	18.4	5.4	0.2	78	205	72,832	4,158	672	163	3.4
2007	9.2	26.5	14.4	2.2	76	210	82,154	4,311	720	120	3.5
2008	57.8	27.4	30.2	10.8	85	219	92,874	6,068	817	266	2.0
2009	21.2	14.7	63.1	15.2	117	204	98,211	6,514	794	143	3.0
2010	36.5	49.1	34.2	6.1	72	230	70,769	5,979	643	132	2.1
2011	30.4	29.7	44.6	17.8	92	221	116,398	6,177	815	220	2.5
2012	20.7	47.4	32.0	13.9	88	205	77,313	3,932	661	196	3.6
2013	10.9	45.6	23.2	7.8	59	221	49,926	4,171	666	105	3.6
2014	5.1	65.3	25.9	24.0	125	204	98,318	5,586	782	269	3.0
2015	38.0	7.9	18.0	8.7	91	183	64,416	4,097	633	121	4.6
2016	61.7	35.1	23.6	5.8	94	195	72,595	4,857	656	137	3.9
2017	45.8	10.2	19.7	6.4	91	205	104,197	5,344	774	163	3.7
2018	30.1	53.2	28.0	17.4	110	198	142,105	7,130	846	167	3.4
2019	17.3	35.7	44.5	20.7	105	190	97,057	5,834	643	164	2.7
2020	20.7	75.6	60.6	17.2	109	205	113,908	6,873	685	254	3.0
2021	22.8	46.6	45.5	26.4	95	187	83,459	4,385	575	193	3.8
2022	14.3	16.6	45.6	26.7	119	180	97,327	5,377	692	221	3.8
2023	18.7	50.4	1.0	36.4	119	193	97,500	6,047	789	196	2.9
2024	19.1	55.0	45.4	23.3	101	187	74,082	5,048	604	115	4.3

Table S2. Complete first-differenced (detrended) vegetation, hydrologic, and climatic data for the Middle Fork Rock Creek watershed, Montana. For this table, vegetation and temperature values have been rounded to the nearest tenth, and flow duration, start day, volumes, precipitation, and snow-water equivalent to the nearest whole number.

Time	June Veg (%)	July Veg (%)	Aug Veg (%)	Sept Veg (%)	High Flow Duration (days)	High Flow Start (# day)	Total Volume (AF)	Baseflow Volume (AF)	Precipitation (mm)	SWE (mm)	Temperature (℃)
1	-30.6	-9.0	-19.5	-8.1	-4	-29	-26,713	-1,102	-126	-73	-0.6
2	7.5	25.1	27.6	16.1	39	-18	29,890	1,363	95	20	1.4
3	-3.3	-11.2	-29.3	-23.5	-57	28	-41,964	-2,754	-236	-57	1.5
4	-0.4	-22.3	-17.8	3.3	12	-5	-254	-386	41	29	-0.3
5	1.6	29.9	-4.7	1.0	20	1	12,309	1,927	145	24	-0.3
6	-36.7	-14.2	-3.3	17.5	-1	-4	8,522	16	-73	-1	0.5
7	9.8	-5.7	17.6	-3.6	-20	29	-1,826	-346	-2	-29	-0.9
8	-5.4	12.8	-17.6	-20.1	-7	-15	-23,045	-878	-75	-90	1.0
9	10.1	-9.9	35.4	10.6	43	11	21,337	3,737	244	10	-2.2
10	-3.0	1.4	-11.7	-9.7	-27	-21	-6,552	-3,055	-341	40	2.2
11	20.8	-11.5	7.6	5.0	14	16	30,559	2,160	313	-26	-1.2
12	-12.5	12.3	-12.0	5.7	19	-25	22,709	-1,033	49	215	0.1
13	-19.8	3.5	20.5	-1.4	6	9	16,285	1,303	97	-161	0.3
14	7.9	16.2	3.3	-0.5	-17	8	-33,983	-324	-172	5	0.9
15	37.3	-29.3	-41.6	2.5	11	-8	1,479	-685	-83	-49	-0.7
16	0.7	-12.5	13.4	-11.4	-42	4	-48,119	-2,100	-192	-17	1.3
17	-26.9	-12.5	-4.0	1.0	21	5	2,589	681	42	-2	-0.7
18	-1.4	46.6	25.0	6.5	-25	16	15,871	457	118	-48	-0.4
19	-0.6	-20.1	-16.1	-8.7	11	-22	3,746	-767	23	105	1.2
20	11.2	11.8	10.1	6.9	4	6	-13,422	1,136	68	-91	-0.7
21	26.2	-0.7	-0.6	-4.1	-15	9	-1,256	-1,104	-178	9	0.4
22	-35.5	-19.5	-23.9	-2.6	9	-15	13,421	-64	97	20	0.2
23	-9.8	8.1	9.0	2.0	-2	5	9,322	153	48	-43	0.2
24	48.5	1.0	15.8	8.6	9	9	10,720	1,758	96	146	-1.5
25	-36.5	-12.7	32.9	4.4	32	-15	5,337	445	-23	-123	1.0
26	15.2	34.4	-28.9	-9.1	-45	26	-27,441	-534	-151	-11	-0.9
27	-6.1	-19.3	10.4	11.6	20	-9	45,628	198	172	88	0.4
28	-9.7	17.7	-12.6	-3.8	-4	-16	-39,085	-2,245	-154	-24	1.1
29	-9.8	-1.9	-8.8	-6.2	-29	16	-27,387	239	4	-92	0.0
30	-5.9	19.8	2.7	16.3	66	-17	48,392	1,415	116	165	-0.6
31	32.9	-57.4	-7.9	-15.4	-34	-21	-33,901	-1,489	-149	-148	1.6
32	23.6	27.2	5.6	-2.9	3	12	8,179	760	23	16	-0.7
33	-15.9	-25.0	-3.8	0.6	-3	10	31,602	487	118	26	-0.2
34	-15.6	43.0	8.2	11.0	19	-7	37,908	1,786	72	4	-0.3
35	-12.8	-17.5	16.5	3.3	-5	-8	-45,048	-1,296	-202	-3	-0.7
36	3.4	39.9	16.1	-3.5	4	15	16,851	1,039	41	90	0.3
37	2.1	-29.0	-15.2	9.2	-14	-18	-30,449	-2,488	-110	-61	0.8
38	-8.5	-30.0	0.2	0.4	24	-7	13,867	992	117	28	0.0
39	4.4	33.8	-44.6	9.7	0	13	173	669	97	-25	-0.9
40	0.4	4.5	44.4	-13.1	-18	-6	-23,418	-998	-185	-81	1.4

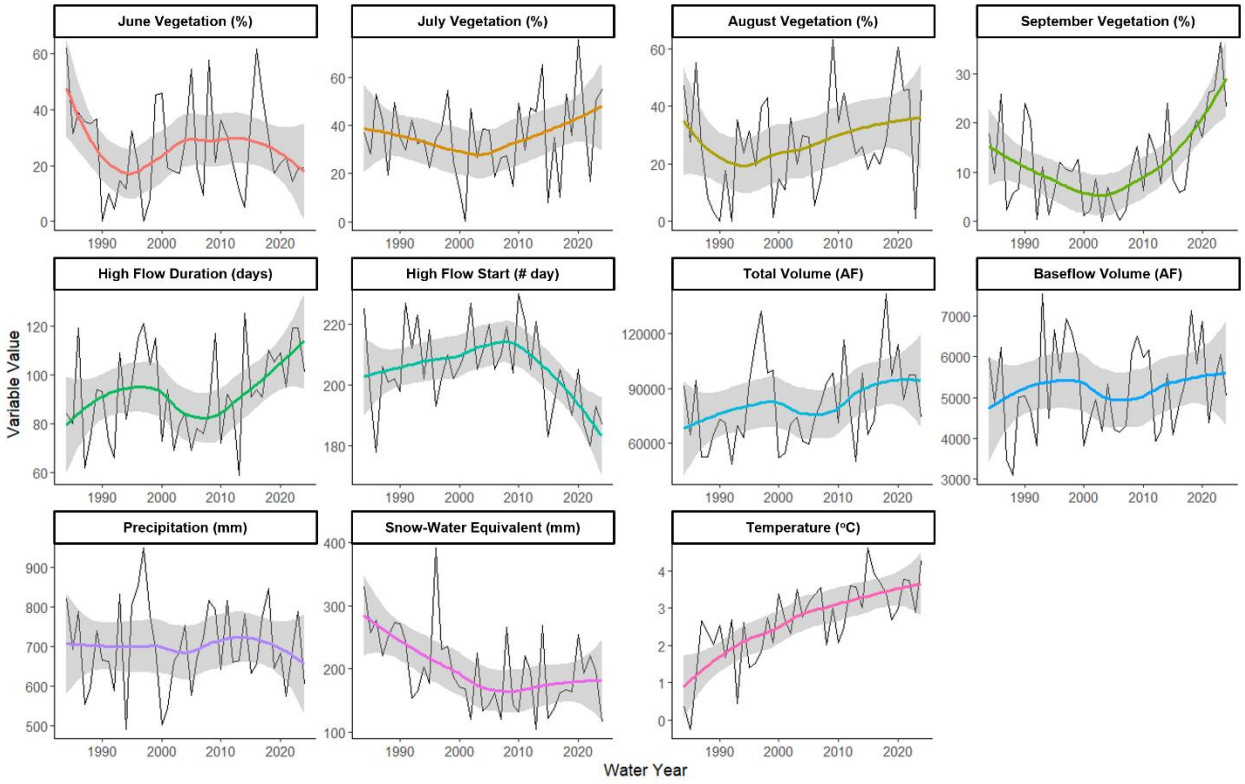

Figure S5. Time series plots of observed variables by water year with LOESS-smoothed trends.

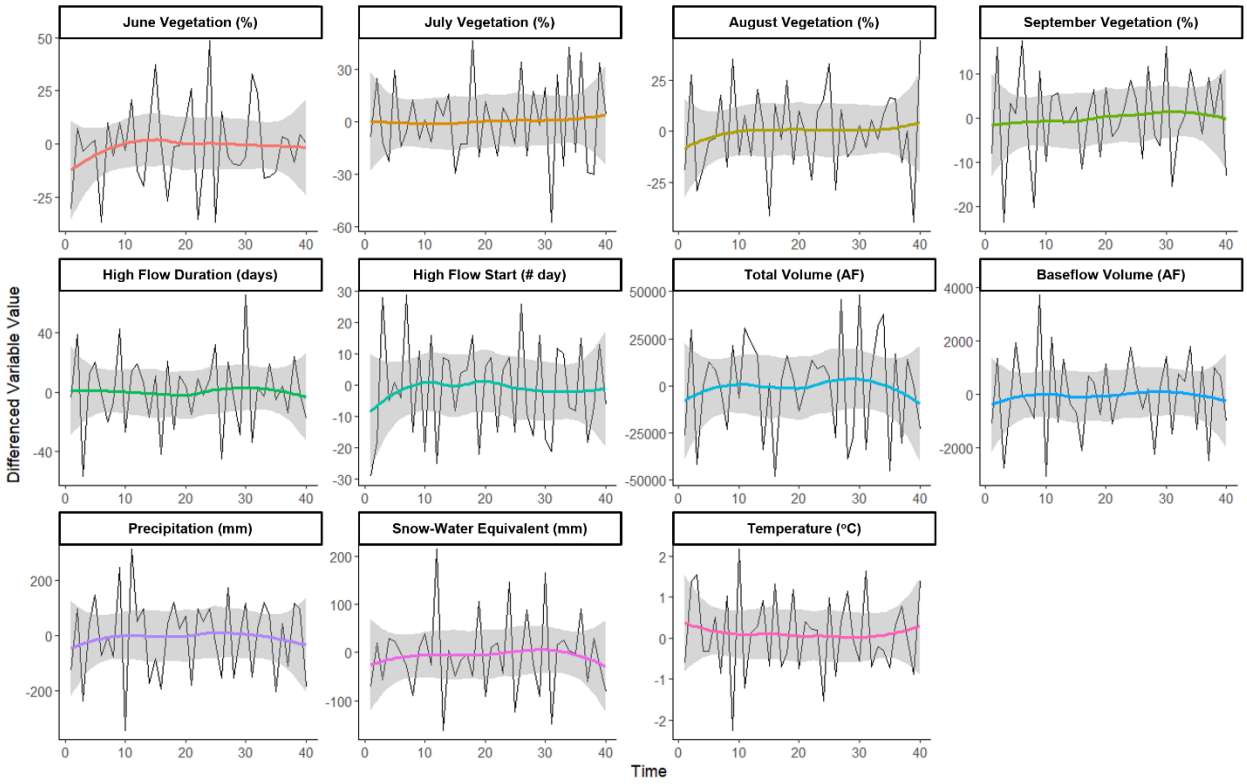

Figure S6. Time series plots of detrended variables with LOESS-smoothed trends.